Metal–Metal Bonding in Transition-Metal Clusters with Open d Shells: Pt_3

Hua Wang and Emily A. Carter*

Department of Chemistry and Biochemistry, University of California, Los Angeles, California 90024-1569
(Received: February 8, 1991; In Final Form: August 6, 1991)

Ab initio generalized valence bond with configuration interaction calculations have been performed for low-lying electronic states of Pt_3. The calculations utilize the relativistic effective core potential developed by Hay and Wadt. Under the constraint of C_{2v} symmetry, seven states derived from three d^9s^1-like Pt atoms ($^3A_1$, $^5B_2$, $^5A_1$, $^5A_2$, $^3B_1$, $^3A_2$, and $^5B_1$) are predicted to have geometries slightly distorted from equilateral triangles, while two other states involving one d^{10}-like Pt and two d^9s^1-like Pt atoms ($^1A_1$ and $^3B_2$) retain equilateral triangle geometries without distortion. Only one low-lying electronic state ($^5\Delta_g$) has a linear geometry, arising from all three Pt atoms in d^9s^1 states. All 10 states are predicted to lie within 6.6 kcal/mol of each other. Other states are found to be at least 10 kcal/mol higher in energy than the ground state ($^3A_1$). The calculated high density of electronic states and the presence of a low-lying linear structure provide some insight into the experimental spectra of platinum trimer. The role of s–s bonding versus d–d bonding in the formation of the Pt_3 cluster is discussed, with the major conclusion that s–s bonding is dominant, while d–d electronic interactions are far less important. However, d–d electronic coupling has a small contribution to the geometric distortion away from an equilateral triangle. Finally, we predict that the Pt_3 ground state is bound by at least 50.3 kcal/mol with respect to three separated ^3D Pt atoms.

I. Introduction

Recently, considerable interest has evolved in determining the properties and reactivities of metal clusters, both experimentally and theoretically. Much of the work has been reviewed previously,[1-5] where transition-metal (TM) clusters are of special interest because of the possibility of d–d bonding. However, detailed electronic and vibrational structural investigations on TM clusters have thus far been limited to dimers and a few trimers and tetramers because experimental and theoretical information about TM trimers and higher clusters are difficult to obtain. Even for TM dimers, there room for improvement in current theoretical descriptions because the d–d correlation problem is extremely severe.

A number of TM trimers, including Sc_3,[6-8] Y_3,[6-8] Cr_3,[9,10] Mn_3,[11] Fe_3,[12] Ni_3,[12-15] Pd_3,[15,16] and Pt_3[15,17,18] have been examined using several experimental techniques and theoretical methods. The presence of open d shells and near degeneracies in $d^{n-2}s^2$ and $d^{n-1}s^1$ atomic states for TMs makes it likely that many molecular electronic states may also be close in energy and s–d orbital mixing may be important. Early TM trimers exhibit extensive d–d bonding,[8] while coinage metal trimers with their filled d shells have little d–d interaction.[33,35] Late TM trimers with open d shells pose interesting questions as to whether d–d bonding will be as important as for early TM trimers. It is likely that d–d interactions will be less dominant in late TMs, since the d orbitals in late TMs are considerably smaller than in early TMs.

Since group 10 aggregates of Ni, Pd, and Pt are employed as catalysts in many industrial processes, understanding their electronic structures are of particular interest. Although comparatively thorough investigations have been carried out for Ni_3,[13,15] the geometric and electronic structures are still somewhat controversial. Walch's calculations on Ni_3[13] provide the most comprehensive picture and are in the best agreement with various experiments. Pd_3 has been characterized a bit less extensively: Lineberger and co-workers[15] have measured the negative ion photoelectron spectrum of Pd_3^- (an experiment that contains information about the electronic structure of both the neutral final state and the anionic initial state), and Balasubramanian[16] has carried out relativistic CI calculations on neutral Pd_3.

Experimental work to determine electronic properties of Pt trimers has been limited to three studies. In the same study where they examined Ni_3^- and Pd_3^-, Lineberger and co-workers also measured the photoelectron spectrum of Pt_3^-.[15] Although the spectrum is quite uncluttered, the transitions were difficult to assign to either purely vibronic or purely electronic transitions to a dense manifold of neutral Pt_3. However, they suggested that a spectrum of such relative simplicity (compared to the broader spectrum observed for Ni_3^-) may indicate the presence of only a few low-lying electronic states. More recently, Eberhardt et al. measured valence electron and 4f core-level photoemission spectra for several platinum clusters deposited on an SiO_2 substrate.[17] On the basis of their Pt trimer spectra, they proposed that linear and triangular structures of Pt_3 may be energetically competitive, similar to Walch's theoretical prediction for Ni_3. Most recently, scanning tunneling microscopy (STM) of small platinum clusters on highly oriented pyrolytic graphite were carried out by Müller et al.[18] They found only two kinds of adsorbed Pt trimers, either linear chains or equilateral triangles with average bond lengths of 2.66 ± 0.32 Å.

Until now, little theoretical effort has focused on Pt_3, although relativistic CI calculations including spin–orbit coupling are in progress by Balasubramanian.[19] Our relativistic CI calculations that do not include spin–orbit effects should be an important reference system for his calculations. A Hartree–Fock pseudo-

(1) Weltner Jr., W.; Van Zee, R. J. In *Comparison of Ab Initio Quantum Chemistry with Experiment for Small Molecules*; Bartlett, R. J., Ed.; Reidel: Dordrecht, 1985; p 1.
(2) Walch, S. P.; Bauschlicher Jr., C. W. In *Comparison of Ab Initio Quantum Chemistry with Experiment for Small Molecules*; Bartlett, R. J., Ed.; Reidel: Dordrecht, 1985; p 17.
(3) Weltner Jr., W.; Van Zee, R. J. *Annu. Rev. Phys. Chem.* **1984**, *35*, 291.
(4) Morse, M. D. *Chem. Rev.* **1986**, *86*, 1049.
(5) Kappes, M. M. *Chem. Rev.* **1988**, *88*, 369.
(6) Knight Jr., L. B.; Woodward, R. W.; Van Zee, R. J.; Weltner Jr., W. *J. Chem. Phys.* **1983**, *79*, 5820.
(7) Moskovits, M.; DiLella, D. P.; Limm, W. *J. Chem. Phys.* **1984**, *80*, 626.
(8) Walch, S. P.; Bauschlicher Jr., C. W. *J. Chem. Phys.* **1985**, *83*, 5735.
(9) DiLella, D. P.; Limm, W.; Lipson, R. H.; Moskovits, M.; Taylor, K. V. *J. Chem. Phys.* **1982**, *77*, 5263.
(10) Ozin, G. A.; Baker, M. D.; Mitchell, S. A.; McIntosh, D. F. *Angew. Chem., Int. Ed. Engl.* **1983**, *22*, 166.
(11) Bier, K. D.; Haslett, T. L.; Kirkwood, A. D.; Moskovits, M. *J. Chem. Phys.* **1988**, *89*, 6.
(12) Nour, E. M.; Alfaro-Franco, C.; Gingerich, K. A.; Laane, J. *J. Chem. Phys.* **1987**, *86*, 4779.
(13) Walch, S. P. *J. Chem. Phys.* **1987**, *86*, 5082 and references therein.
(14) Woodward, J. R.; Cobb, S. H.; Gole, J. L. *J. Phys. Chem.* **1988**, *92*, 1404.
(15) Ervin, K. M.; Ho, J.; Lineberger, W. C. *J. Chem. Phys.* **1988**, *89*, 4514.
(16) Balasubramanian, K. *J. Chem. Phys.* **1989**, *91*, 307.
(17) Eberhardt, W.; Fayet, P.; Cox, D. M.; Fu, Z.; Kaldor, A.; Sherwood, R.; Sondericker, D. *Phys. Rev. Lett.* **1990**, *64*, 780.
(18) Müller, U.; Sattler, K.; Xhie, J.; Venkateswaran, N.; Raina, G. *J. Vac. Sci. Technol. B* **1991**, *9*, 829.
(19) Balasubramanian, K., private communication.

0022-3654/92/2096-1197$03.00/0

potential study by Gavezzotti et al.[20] yielded a very weakly bound platinum trimer, but no details of the electronic structure or geometric parameters were reported. Semiempirical extended Hückel theory (EHT) calculations on Pt_3 by Bigot and Minot[21] have been carried out on equilateral triangle, linear, and two isosceles triangle (with 90° and 120° apex angles) structures. They concluded that an equilateral triangle with a bulk bond length (R_{Pt-Pt} = 2.77 Å) is the most stable structure and that the Pt_3 atomization energy is 36.0 kcal/mol. However, results from EHT must be considered with caution, since EHT does not distinguish well between various electronic states and is not reliable for predicting geometries or relative energetics.

In the present work, we carried out generalized valence bond with configuration interaction (GVB/CI)[22,23] calculations for Pt_3 and extracted a qualitative description of its electronic spectrum, equilibrium geometries, and metal–metal bond character. In particular, our purpose is to understand the role of valence d electrons versus s electrons in metal–metal bonding. Is s–d mixing important, does s dominate over d or vice versa, and does p-orbital mixing play a role? To compare with previous studies and our Pt trimer results, we also carried out less extensive calculations on Pt atom and Pt dimer. Section II of this paper describes our method of calculation, section III presents and discusses our results, and section IV provides a summary of our conclusions.

II. Calculational Details

The 10 valence electrons of Pt were treated explicitly within the (3s3p3d/3s2p2d) Gaussian basis set of Hay and Wadt, with the core electrons represented by a relativistic effective core potential (RECP).[24a] This RECP accounts for mass–velocity and Darwin terms in the relativisitic Hamiltonian but neglects spin–orbit interactions. Thus, the results presented here may be considered as averaged over J states. However, this RECP properly accounts for the relativistic contraction of orbitals, which is the dominant chemical relativistic effect, since such orbital contractions change the orbital overlaps within bonds and hence affect the intrinsic bond strength and character. This basis set and RECP description has been used successfully in the past to study platinum hydride by Rohlfing et al.[24b]

The equilibrium geometries (obtained point-by-point with interpolation) and self-consistent field (SCF) wave functions for all states of Pt_3 were obtained at the GVB-PP(3/6) level.[22e] GVB-PP(3/6) indicates that three electron pairs are correlated as GVB pairs, with two natural orbitals per pair, for a total of six orbitals. PP stands for perfect pairing, i.e., each pair of electrons is singlet coupled.[22e] Only low-lying electronic states in C_{2v} and $D_{\infty h}$ point groups for the triangular and linear structures, respectively, were considered. In other words, possible geometric minima with all three Pt–Pt distances inequivalent were not examined.

The wave functions of the low-lying states were obtained in the following manner. First, full valence CI calculations within all s and d orbitals [i.e., 30 electrons in 18 orbitals complete active space CI (CAS-CI)] were performed using the self-consistent GVB-PP set of orbitals for one particular state, in order to determine the preferred orbital occupations for each spatial and spin symmetry. We examined all possible singlet, triplet, quintet, and septet states in C_{2v} and D_{2h} symmetry that arise from considering the interaction between three ground state d^9s^1 Pt atoms in an equilateral triangle geometry with a bond length of 2.81 Å. In C_{2v} symmetry, the 18 CAS orbitals consist of seven a_1, three a_2, three b_1, and five b_2 orbitals, with the orbitals taken from the GVB(1/2)-PP $^5B_2$ wave function. In D_{2h} symmetry, the CAS orbitals contain six a_g, two b_{1g}, two b_{2g}, two b_{3g}, one a_u, three b_{1u}, one b_{2u}, and one b_{3u} orbitals, with the orbitals taken from the $^5B_{1g}$ ($^5\Delta_g$) wave function. Once the dominant configurations for each state were identified in this way, we solved for GVB(3/6)-PP wave functions or the equivalent (GVB(1/2)-PP for quintet states, GVB(2/4)-PP for triplets, and GVB(3/6)-PP for singlets) for several orbital occupations of each possible state. Full valence CI calculations were then performed again using the orbitals from these SCF wave functions as the zeroth-order description, in order to check that no bias was built into the first set of CI calculations by using either the $^5B_2$ or $^5B_{1g}$ set of orbitals to search for appropriate occupations. We did not solve for higher roots of all states in C_{2v} and D_{2h} symmetries. Thus, we only give the lowest energy solution for each spin and spatial symmetry and do not rule out the possibility that other states of the same symmetry with different orbital occupations may be low-lying as well.

Several CI calculations were carried out employing these GVB-PP(3/6) wave functions. The simplest extension from GVB-PP, the GVB-RCI(3/6) wave function, allows both single and double excitations within each GVB pair, leading to a total of $3^3 = 27$ configurations. This level of calculation includes all possible spin couplings and interpair correlations in the molecular description. The next extension from RCI is the GVB-CI(3/6) wave function, which includes all possible excitations within the six GVB correlated orbitals. GVB-RCI*SD_{s-s} and GVB-RCI*-$[SD_{s-s} + SD_{d-d}]$ are multireference single and double excitation CIs that use all of the RCI configurations as the reference space. GVB-RCI*SD_{s-s} allows all single and double excitations from the s–s bond and GVB–RCI*$(SC_{s-s} + SD_{d-d})$ allows all single and double excitations from both the s–s and d–d bonds separately. Finally, we also carried out correlation-consistent CI (CCCI) calculations[23,25] for the cohesive energy of the ground $^3A_1$ state, which adds to GVB-RCI*$(SD_{s-s} + SD_{d-d})$ all valence single excitations from the RCI reference states. These theoretical methods have been used in the past to successfully predict both electronic excitation energies and bond dissociation energies in organic and organometallic systems.[23,25] Although this does not necessarily imply success for metal cluster applications, at the very least, these methods are expected to provide approximately correct trends. Unfortunately, no definitive theory yet exists to evaluate the quantitative aspects of metal–metal bonds in a general, reliable fashion.

III. Results and Discussion

(A) Platinum Atom. In Table I, the Pt atomic state splittings for the basis set employed is compared with the experimental and relativistic numerical Hartree–Fock (RNHF) values. RNHF[24] predicts the correct ground state for Pt atom (^3D) but yields poor ^1S–^3D and ^3F–^3D splittings. The lowest level calculation that avoids biases in orbital occupation and in spin coupling involves a GVB-RCI(1/2) on the ^1S state of Pt and open-shell HF calculations on all other states; we group these together as a GVB-RCI(1/2) set of calculations. GVB-RCI(1/2) also calculates the correct ground state and improves the ^3F–^3D splitting (16.0 kcal/mol, compared with the experimental J-averaged value of 14.7 kcal/mol[26]). The ^1S–^3D splitting at the GVB-RCI(1/2) level makes the ^1S state more unstable, leading to a bias against d^{10} character in the wave functions for Pt clusters at this low level of theory.

(B) Platinum Dimer. We carried out two types of investigations on four low-lying electronic states of Pt dimer. One is a complete

(20) Gavezzotti, A.; Tantardini, G. F.; Miessner, H. *J. Phys. Chem.* **1988**, *92*, 872.
(21) Bigot, B.; Minot, C. *J. Am. Chem. Soc.* **1984**, *106*, 6601.
(22) The details of GVB and MCSCF approaches used may be found in: (a) Hunt, W. J.; Dunning Jr., T. H.; Goddard III, W. A. *Chem. Phys. Lett.* **1969**, *3*, 606. (b) Goddard III, W. A.; Dunning Jr., T. H.; Hunt, W. J. *Chem. Phys. Lett.* **1969**, *4*, 231. (c) Hunt, W. J.; Goddard III, W. A.; Dunning Jr., T. H. *Chem. Phys. Lett.* **1970**, *6*, 147. (d) Hunt, W. J.; Hay, P. J.; Goddard III, W. A. *J. Chem. Phys.* **1972**, *57*, 738. (e) Bobrowicz, F. W.; Goddard III, W. A. In *Methods of Electronic Structure Theory*; Schaefer, H. F., Ed.; Plenum: New York, 1977; pp 79–127. (f) Yaffe, L. G.; Goddard III, W. A. *Phys. Rev. A* **1976**, *13*, 1682.
(23) Carter, E. A.; Goddard III, W. A. *J. Chem. Phys.* **1988**, *88*, 3132 and references therein.
(24) (a) Hay, P. J.; Wadt, W. R. *J. Chem. Phys.* **1985**, *82*, 270. (b) Rohlfing, C. M.; Hay, P. J.; Martin, R. L. *J. Chem. Phys.* **1986**, *85*, 1447.
(25) Carter, E. A.; Goddard III, W. A. *J. Chem. Phys.* **1988**, *88*, 1752 and references therein.
(26) Moore, C. E. In *Atomic Energy Levels as Derived From the Analyses of Optical Spectra*; U.S. Government Printing Office: Washington, D.C., 1971; Vol. III, pp 181–185.

TABLE I: Atomic State Splittings of Pt Atom (kcal/mol)

state	ΔE(expt)[a]	ΔE(RNHF)[b]	ΔE[GVB-RCI(1/2)][c]
^1D (d^9s^1)	32.1		23.1
^3F (d^8s^2)	14.7	9.2	16.0
^1S (d^{10})	11.0	20.8	22.3
^3D (d^9s^1)	0.0	0.0	0.0[d]

[a] Experimental values are averaged over J states.[26] [b] Relativistic numerical Hartree–Fock results.[23] [c] GVB-RCI(1/2) results for the ^1S state using the 3s2p2d basis set and the RECP of Hay and Wadt.[23] The corresponding level of calculation for the ^1D, ^3F, and ^3D states is open-shell HF. [d] The total energy of the ^3D state at the open shell HF level is −26.238 10 hartrees.

TABLE II: Properties of Four Electronic States of Pt_2 from CASSCF Calculations[a]

state	MO configuration[b]	R_e,[c] Å	ω_e,[d] cm^{-1}	D_e,[e] kcal/mol
$^3\Pi_u$	$(\pi_g)^3(\delta_u)^3$	2.70	126	23.4
$^1\Gamma_g$	$(\delta_u)^2$	2.72	138	26.6
$^3\Gamma_u$	$(\delta_g)^3(\delta_u)^3$	2.75	169	26.6
$^3\Sigma_g^-$	$(\delta_u)^2$	2.74	161	26.7

[a] Calculated at the 20 electrons in 12 orbitals CASSCF level (see text). [b] Only the characteristic part of the configuration is shown. [c] R_e is the equilibrium bond length in angstroms. [d] ω_e is the harmonic vibrational frequency in wavenumbers. [e] The CASSCF total energy for the $^3\Sigma_g^-$ state is −52.520 45 hartrees.

active space MCSCF (CASSCF) calculation (Table II), where the CAS includes all 20 valence electrons within the 12 valence orbitals arising from two d^9s^1 Pt atoms. All electronic states examined were extremely close in energy (within 3.3 kcal/mol), making it impossible to predict which state is the ground state. The equilibrium bond lengths (R_e) from CASSCF calculations on four electronic states ($^1\Gamma_g$, $^3\Gamma_u$, $^3\Pi_u$, and $^3\Sigma_g^-$) range from 2.70 to 2.75 Å, the vibrational frequencies (ω_e) vary from 126 to 169 cm^{-1}, while the bond dissociation energies (D_e) range from 23.4 to 26.7 kcal/mol at this level of theory. The other set of calculations (Table III) involves the usual multireference CI calculations described in section II, employing a GVB(2/4)-PP zeroth-order wave function. The $^3\Pi_u$ and $^3\Sigma_g^-$ states are unbound in this type of calculation, while the other two states ($^1\Gamma_g$ and $^3\Gamma_u$) are within 1 kcal/mol of each other. The bond lengths optimized at the GVB-PP(2/4) level are found to be also ≅2.7 Å, and the harmonic vibrational frequencies are 162 and 163 cm^{-1}. The dissociation energy of the $^1\Gamma_g$ state at the CCCI level is predicted to be D_e = 37.6 kcal/mol. Mulliken population analysis of the GVB-PP orbitals show that both bound states ($^1\Gamma_g$ and $^3\Gamma_u$) have both Pt atoms in the ground d^9s^1 atomic state.

Several experiments on Pt dimer have provided values for $R_e(Pt_2)$, $\omega_e(Pt_2)$, and $D_0(Pt_2)$. Müller et al. used STM to estimate the average bond length of Pt_2 on graphite to be 2.45 ± 0.26 Å,[18] in reasonable agreement with our theoretical predictions. Gingerich and co-workers[27,28] studied the gas-phase Pt dimer to arrive first at an empirical estimate for $D_0(Pt_2)$ of 66.4 ± 6.0 kcal/mol,[27] followed by high-temperature equilibrium studies[28] that yielded $D_0(Pt_2)$ = 85.6 ± 14.3 kcal/mol from second-law analysis. With assumptions about the ground state, the bond length, and the vibrational frequency, the third-law evaluation gave $D_0(Pt_2)$ = 85.6 ± 3.7 kcal/mol. Most recently, Morse and co-workers used resonant two-photon ionization spectroscopy to study jet-cooled Pt dimers.[29] Their measurements placed the dissociation energy of Pt_2 at 72.4 ± 0.5 kcal/mol and the vibrational frequencies of excited Pt_2 between 140 and 195 cm^{-1}, in excellent agreement with our calculations. However, our predicted bond strength is nearly a factor of 2 smaller than this most recent experimental value. The discrepancy between theory and experiment remains to be resoived. It may be possible that the experiment is accessing a different manifold of states than the theory or that correlation and relativistic effects are simply extremely severe. At any rate, the CCCI results are in closer agreement with experiment than the CASSCF results, suggesting the former method to be more reliable for use on Pt_3.

Two ab initio investigations of the electronic states of Pt dimer have been reported. Basch et al. performed singly correlated bond pair SCF calculations on the same four $^1\Gamma_g$, $^3\Gamma_u$, $^3\Pi_u$ and $^3\Sigma_g^-$ states that we examined at the CASSCF level.[30] The most strongly bound electronic state among them was the $^1\Gamma_g$ state, consistent with our results in Table III, but with a predicted $D_0(Pt_2)$ = 21.4 kcal/mol, much smaller than our predicted D_0 of 37.6 kcal/mol (Table III). The bond lengths of the four states were predicted to be 2.51–2.63 Å, similar to our predictions, while the vibrational frequencies were somewhat higher (225–271 cm^{-1}). Balasubramanian carried out CASSCF/FOCI (first order CI) calculations on low-lying electronic states of Pt_2.[31] By contrast, the $^3\Pi_u$ state was predicted to be the lowest, with the $^3\Sigma_g^-$ state almost nearly degenerate, while the $^1\Gamma_g$ and $^3\Gamma_u$ states were 7.8 and 8.2 kcal/mol higher. The bond lengths were found to be 2.4–2.6 Å for all low-lying electronic states, somewhat shorter than those predicted here. The vibrational frequencies ranged from 170 to 306 cm^{-1}, in reasonable agreement with our results. In the absence of spin–orbit interaction, the dissociation energy for the $^3\Pi_u$ state was predicted to be 53.0 kcal/mol. However, in the presence of spin–orbit interaction, the bond energy dropped to D_e(Pt–Pt) = 45.0 kcal/mol and the ordering of electronic states changed completely.

In summary, the theoretical calculations seem to predict bond lengths similar to experiment but smaller values for the bond energy. However, only a few experiments and calculations have been carried out, and no general consensus has been reached. Clearly, more effort is needed to reach quantitative agreement between experiment and theory on Pt_2, but this is beyond the scope of this paper. However, if the experiments are correct, we suggest that predicted geometries for Pt_3 may be reasonable, while predicted Pt_3 atomization energies from CCCI calculations will be lower bounds.

(C) Platinum Trimer. Table IV summarizes the dominant GVB-PP configurations for the 10 lowest lying electronic states of each symmetry at their optimum geometries. Each bond pair has two natural orbitals and a net population of two electrons. GVB pairs involving orbitals with high overlap consist of nearly doubly occupied first natural orbitals (e.g., 1.96–1.97 electrons) and nearly empty second natural orbitals (e.g., 0.03–0.04 electron). Low overlap bond pairs have both natural orbitals nearly singly occupied (e.g., 1.07 and 0.93 in each). Thus, the $^1A_1$ state has two high-overlap electron pairs and one low overlap electron pair. All of the triplet states except $^3B_2$ each have one pair with high overlap and one with little overlap, and all of the quintet states have one pair with high overlap. These trends are due to characteristic s–s and d–d bonds, as explained below.

Initially, we examined the Pt_3 electronic state spectrum for the bulk geometry, i.e., an equilateral triangle with a bulk bond length of R_{Pt-Pt} = 2.77 Å. Among all possible singlet, triplet, quintet, and septet states in C_{2v} symmetry, the $^1A_2$, $^1B_1$ and $^1B_2$ states (which are open-shell singlet states) are found to be higher in energy by at least 10 kcal/mol at the GVB-PP level. Since they are always more unstable than their corresponding triplet states (with the same electron configuration), they are unlikely to be among the lowest lying electronic states and were not studied further. The results from five levels of calculation for the nine lowest lying electronic states of each symmetry are given in Table V. What we find is at first glance quite surprising. While it seems sensible that the $^7A_1$ state with all six open-shell electrons unpaired (i.e., it has no metal–metal bonds) is unbound at the GVB-CI level by 14.9 kcal/mol relative to three ground-state ^3D Pt atoms, we find that nine states ($^1A_1$, $^3A_1$, $^5B_2$, $^5A_1$, $^3B_2$, $^3A_2$, $^3B_1$, $^5B_1$, and

(27) Miedema, A. R.; Gingerich, K. A. *J. Phys. B* **1979**, *12*, 2081.
(28) Gupta, S. K.; Nappi, B. M.; Gingerich, K. A. *Inorg. Chem.* **1981**, *20*, 966.
(29) Taylor, S.; Lemire, G. W.; Hamrick, Y. M.; Fu, Z.; Morse, M. D. *J. Chem. Phys.* **1988**, *89*, 5517.
(30) Basch, H.; Cohen, D.; Topiol, S. *Isr. J. Chem.* **1980**, *19*, 233.
(31) Balasubramanian, K. *J. Chem. Phys.* **1987**, *87*, 6573.

TABLE III: Equilibrium Properties for Two Low-Lying States of Pt_2 from GVB/CI Calculations

state	R_e,[a] Å	ω_e,[a] cm^{-1}	ΔE, kcal/mol PP[b]	RCI[c]	GVB-CI[d]	RCI*SD_s[e]	RCI*$SD_{s,d}$[f]	D_e, kcal/mol RCI*$SD_{s,d}$[g]	CCCI[h]
$^3\Gamma_u$	2.67	163	0.2	1.0	0.7	0.6	0.6	23.9	36.1
$^1\Gamma_g$	2.71	162	0.0	0.0	0.0	0.0	0.0	24.6	37.6
			(−52.509 49)[i]	(−52.510 80)[i]	(−52.510 80)[i]	(−52.518 35)[i]	(−52.519 34)[i]		

[a] R_e is the bond length in angstroms; ω_e is the harmonic vibrational frequency in wavenumbers. [b] PP stands for GVB-PP(3/6). [c] RCI stands for GVB-RCI(3/6). [d] GVB-CI stands for GVB-CI(3/6). [e] RCI*SD_s stands for GVB-RCI(3/6)*SD_{s-s}. [f] RCI*$SD_{s,d}$ stands for GVB-RCI(3/6)*-[SD_{s-s}+SD_{d-d}]. [g] Adiabatic bond dissociation energy at the RCI*$SD_{s,d}$ level. [h] Adiabatic bond dissociation energy at the CCCI (RCI*$SD_{s,d}$ + RCI*S_{val}) level. The CCCI total energy for $^1\Gamma_g$ Pt_2 is −52.540 07 hartrees and the corresponding HF*S_{val} total energy for Pt atom (d^9s^1) is −26.240 09 hartrees. [i] The total energy in hartrees is given in parentheses underneath ΔE for the ground state at each level of calculation.

TABLE IV: Orbital Occupancies for the 10 Lowest-Lying States of Each Symmetry for Pt_3 in Their Optimum Geometries at the GVB-PP Level[a]

state	orbital occupancies[b]																	
C_{2v}	$1a_1$	$2a_1$	$3a_1$	$4a_1$	$5a_1$	$6a_1$	$7a_1$	$1a_2$	$2a_2$	$3a_2$	$1b_1$	$2b_1$	$3b_1$	$1b_2$	$2b_2$	$3b_2$	$4b_2$	$5b_2$
$^1A_1$	2.00	2.00	2.00	1.97	1.96*	1.06	0.03	2.00	2.00	2.00	2.00	2.00	2.00	2.00	2.00	2.00	0.94	0.04
$^3A_1$	2.00	2.00	2.00	1.97*	1.08	1.00	1.00	2.00	2.00	2.00	2.00	2.00	2.00	2.00	2.00	2.00	0.92	0.03
$^3A_2$	2.00	2.00	2.00	2.00	1.97*	1.07	1.00	2.00	2.00	1.00	2.00	2.00	2.00	2.00	2.00	2.00	0.93	0.03
$^3B_1$	2.00	2.00	2.00	2.00	1.97*	1.07	1.00	2.00	2.00	2.00	2.00	2.00	1.00	2.00	2.00	2.00	0.93	0.03
$^3B_2$	2.00	2.00	2.00	1.97	1.96*	1.00	0.03	2.00	2.00	2.00	2.00	2.00	2.00	2.00	2.00	2.00	1.00	0.04
$^5A_1$	2.00	2.00	2.00	1.97*	1.00	1.00	0.03	2.00	2.00	2.00	2.00	2.00	2.00	2.00	2.00	2.00	1.00	1.00
$^5A_2$	2.00	2.00	2.00	2.00	1.97*	1.00	1.00	2.00	2.00	2.00	2.00	2.00	1.00	2.00	2.00	2.00	1.00	0.03
$^5B_1$	2.00	2.00	2.00	2.00	1.97*	1.00	1.00	2.00	2.00	1.00	2.00	2.00	2.00	2.00	2.00	2.00	1.00	0.03
$^5B_2$	2.00	2.00	2.00	1.97*	1.00	1.00	1.00	2.00	2.00	2.00	2.00	2.00	2.00	2.00	2.00	2.00	1.00	0.03
$D_{\infty h}$	$1\sigma_g$	$2\sigma_g$	$3\sigma_g$	$4\sigma_g$	$1\pi_g$	$2\pi_g$	$3\pi_g$	$4\pi_g$	$1\delta_g$	$2\delta_g$	$3\delta_g$	$4\delta_g$	$1\sigma_u$	$2\sigma_u$	$1\pi_u$	$2\pi_u$	$1\delta_u$	$2\delta_u$
$^5\Delta_g$	2.00	2.00	1.99*	0.01	2.00	2.00	2.00	2.00	2.00	2.00	1.00	1.00	2.00	1.00	2.00	2.00	2.00	1.00

[a] This does not exclude the possibility that other states of the same symmetry with different orbital occupations may also be low-lying (see text). [b] Asterisks are shown next to the occupations for primarily s-like orbitals.

TABLE V: Relative Energies (kcal/mol) for Low-Lying States of Pt_3 in the Bulk Geometry (θ = 60.0° and R_{Pt-Pt} = 2.77 Å)

state	ΔE, kcal/mol PP[a]	RCI[b]	GVB-CI[c]	RCI*SD_s[d]	RCI*$SD_{s,d}$[e]
$^5A_2$	1.9	1.9	2.2	6.5	7.1
$^5B_1$	1.9	1.9	2.2	6.5	7.1
$^3B_1$	3.2	2.2	2.4	3.0	2.9
$^3A_2$	3.1	2.1	2.1	2.6	2.4
$^3B_2$	1.6	1.5	1.7	1.9	2.2
$^5A_1$	0.7	0.6	1.3	0.9	1.1
$^5B_2$	0.0 (−78.755 87)[f]	0.01	0.3	0.8	0.8
$^3A_1$	1.0	0.03	0.0 (−78.757 49)[f]	0.7	0.4
$^1A_1$	1.1	0.0 (−78.755 89)[f]	0.5	0.0 (−78.765 80)[f]	0.0 (−78.766 76)[f]

[a] PP stands for GVB-PP(3/6). [b] RCI stands for GVB-RCI(3/6). [c] GVB-CI stands for GVB-CI(3/6). [d] RCI*SD_s stands for GVB-RCI(3/6)-*SD_{s-s}. [e] RCI*$SD_{s,d}$ stands for GVB-RCI(3/6)*[SD_{s-s}+SD_{d-d}]. [f] The total energy in hartrees is given in parentheses underneath ΔE for the ground state at each level of calculation.

$^5A_2$) are within 7.1 kcal/mol of the ground state for all five calculational levels. Indeed, three states lie within 0.8 kcal/mol of each other, with the $^1A_1$ state lowest in energy for the equilateral triangle at the highest level of theory. Increasing the level of electron correlation increases the energy splittings, from a spread of only 3.2 kcal/mol at the GVB-PP(3/6) level to a range of 7.1 kcal/mol at the GVB-RCI*[SD_{s-s} + SD_{d-d}] level. This dense electronic spectrum is at variance with the intuitive notion that the large 5d orbitals of third-row TMs (relative to first- and second-row TMs) should yield high d–d orbital overlap that would favor more spin pairing and therefore fewer low-lying states of high spin multiplicity than Ni_3, for example.

The physical reason for the high density of states of different spin lying so close to the $^1A_1$ ground state becomes clear when one examines the nature of the orbitals involved in intracluster bonding. The dominant feature holding the cluster together is a bond involving primarily the three Pt 6s orbitals (one Pt atom contributes considerably less than the other two Pt atoms), which is present for all low-lying states except for the $^7A_1$ state. This bond is reasonably strong, as indicated by both the size of the orbital overlap (S_{s-s} = 0.76) and the predicted Pt_3 cohesive energy (≥50 kcal/mol, vide infra). The quintet states only have this single s–s bond holding the cluster together, the triplet states each have this s–s bond and also a d–d intracluster bond, while the $^1A_1$ state has both s–s and d–d bonds and effectively one d^{10} Pt atom as well. To illustrate this point more clearly, we show the three types of bonding pairs characteristic of all the quintet, triplet, and singlet states in Figure 1. In contrast to the nature of the s–s bond, the d–d bond is nearly worthless, as evidenced by the near degeneracy of the $^3A_1$ (s–s plus d–d bonding) and the $^5B_2$ (s–s bonding only) states and the negligible orbital overlap in the d–d bond (S_{d-d} = 0.03). Essentially, core–core and valence d–d repulsions force the metal–metal bond distances to be long enough such that the d orbitals on different metal centers are only weakly interacting, resulting in very small energy differences between states that only differ by high versus low spin coupling of the open-shell d orbitals. Indeed, all group 10 metals have small d orbitals compared to early TMs, which leads to the conclusion that Ni, Pd, and Pt clusters may all exhibit dense electronic spectra.

In the process of optimizing the structure of Pt_3, we examined first equilateral triangle geometries, then isosceles triangles and finally linear structures. Table VI lists the optimized bond lengths and state splittings for the equilateral triangle structures. We find that the $^1A_1$ state has the shortest bond length at 2.79 Å

TABLE VI: Relative Energies (kcal/mol) and Optimized Bond Lengths (Å) for the Lowest-Lying States of Pt_3 in Equilateral Triangle Geometries

state	R_e,[a] Å	ΔE, kcal/mol PP[b]	RCI[c]	GVB-CI[d]	RCI*SD_s[e]	RCI*$SD_{s,d}$[f]
$^5B_1$	2.86	1.9	2.1	2.2	6.3	7.0
$^5A_2$	2.86	1.9	2.1	2.3	6.2	6.9
$^3B_2$	2.81	2.7	2.8	3.0	2.3	2.5
$^3B_1$	2.86	3.0	2.0	2.2	2.2	2.3
$^3A_2$	2.86	3.1	2.1	2.1	2.0	2.0
$^1A_1$	2.79	2.4	1.4	2.1	1.1	1.2
$^5A_1$	2.84	1.0	0.9	1.7	0.4	0.8
$^5B_2$	2.86	0.0 (−78.758 11)[g]	0.2	0.4	0.3	0.4
$^3A_1$	2.86	1.0	0.0 (−78.758 41)[g]	0.0 (−78.760 24)[g]	0.0 (−78.767 85)[g]	0.0 (−78.769 05)[g]

[a] R_e is the bond length. [b] PP stands for GVB-PP(3/6). [c] RCI stands for GVB-RCI(3/6). [d] GVB-CI stands for GVB-CI(3/6). [e] RCI*SD_s stands for GVB-RCI(3/6)*SD_{s-s}. [f] RCI*$SD_{s,d}$ stands for GVB-RCI(3/6)*[SD_{s-s}+SD_{d-d}]. [g] The total energy in hartrees is given in parentheses underneath ΔE for the ground state at each level of calculation.

TABLE VII: Equilibrium Properties for Low-Lying States of Pt_3

state	R_e,[a] Å	θ_e,[b] deg	ΔE,[c] kcal/mol PP[d]	RCI[e]	GVB-CI[f]	RCI*SD_s[g]	RCI*$SD_{s,d}$[h]	D_e, kcal/mol RCI*$SD_{s,d}$[i]	CCCI
$^5B_1$	2.96	54.9	1.6	2.0	2.1	5.8	6.6	29.5	
$^5A_2$	2.98	54.6	1.6	2.0	2.1	5.8	6.6	29.5	
$^5\Delta_g$	2.77	180.0	5.8	3.2	4.2	5.7	5.7	30.4	
$^3B_2$	2.81	60.0	4.6	5.0	5.0	4.0	4.2	31.9	
$^1A_1$	2.79	60.0	4.4	3.5	4.0	2.7	2.9	33.1	
$^3B_1$	2.97	54.7	2.6	1.8	1.9	1.9	2.0	34.1	
$^3A_2$	2.97	54.8	2.6	1.8	1.8	1.7	1.7	34.3	
$^5A_1$	2.79	65.0	1.7	1.8	2.5	0.7	1.2	34.9	
$^5B_2$	2.95	55.5	0.0 (−78.761 16)[j]	0.4	0.5	0.4	0.5	35.5	
$^3A_1$	2.97	54.6	0.8	0.0 (−78.761 78)[j]	0.0 (78.763 39)[j]	0.0 (−78.770 43)[j]	0.0 (−78.771 77)[j]	36.1	50.3[k]

[a] R_e is the apex Pt to base Pt bond length. [b] θ_e is the apex angle. [c] Relative energies in kcal/mol at various levels of electron correlation. [d] PP stands for GVB-PP(3/6). [e] RCI stands for GVB-RCI(3/6). [f] GVB-CI stands for GVB-CI(3/6). [g] RCI*SD_s stands for GVB-RCI(3/6)*SD_{s-s}. [h] RCI*$SD_{s,d}$ stands for GVB-RCI(3/6)*[SD_{s-s}+SD_{d-d}]. [i] Atomization energy at the RCI*$SD_{s,d}$ level. [j] The total energy in hartrees is given in parentheses underneath ΔE for the ground state at each level of calculation. [k] The atomization energy at the CCCI (RCI*$SD_{s,d}$ + RCI*S_{val}) level. The CCCI total energy for Pt_3 is −78.800 38 hartrees and the corresponding HF*S_{val} total energy for Pt atom (d^9s^1) is −26.240 09 hartrees.

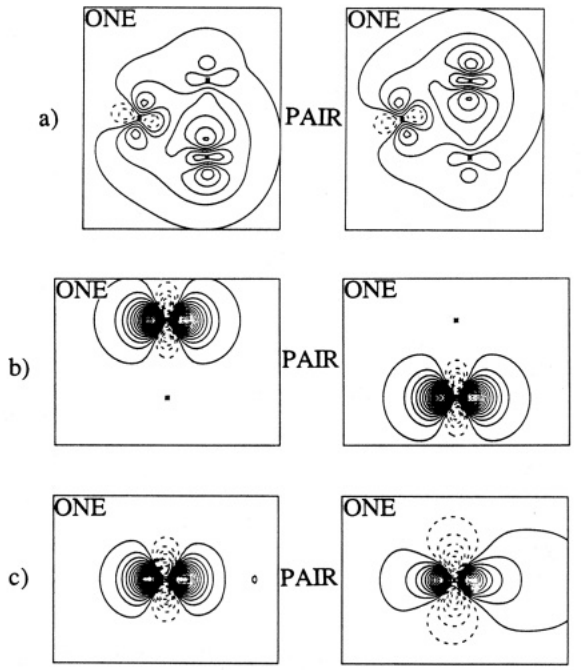

Figure 1. GVB one-electron orbitals for the $^1A_1$ state at its optimum geometry: (a) the 6s–6s bond pair (overlap = 0.76); (b) the 5d–5d bond pair (overlap = 0.03); (c) the 5d lone pair (overlap = 0.79). Contours range from −0.50 to 0.50 au, at intervals of 0.03 au.

(similar to R_{bulk} = 2.77 Å), consistent with the idea that maximum spin pairing favors maximum orbital overlap (achieved for the shortest bond lengths). All higher spin states exhibit considerably longer bonds because of the repulsion between orbitals of the same spin. Table VI suggests that merely relaxing the bulk bond length constraint yields little change in the density of electronic states, which still lie within 7.0 kcal/mol of each other.

We then examined whether linear or isosceles triangle geometries were preferred over equilateral structures for each state, because the 6s electron configuration $(a_1)^2(e)^1$ should lead to a Jahn–Teller distortion, analogous with Ni_3,[13] Na_3,[32] Ag_3,[33-35] and Cu_3.[35-39] We expected that since Pt's 5d orbitals are relatively large, relaxation of the rigid equilateral triangle might favor high d–d bond overlaps and lead to significantly shorter bonds, a low-spin ground-state, and a sparser spectrum of low-lying excited states. However, our results described below indicate that this is not the case.

Table VII shows the predicted equilibrium properties for 10 low-lying states of Pt_3. We find that the energy splitting still remains in the 7 kcal/mol range upon relaxing the D_{3h} symmetry constraint. The $^3A_1$ and $^5B_2$ states stay nearly degenerate at all levels of theory, making it impossible to predict which of these two states is the actual ground state. In fact, many electronic states with different numbers of intracluster bonds still lie close energetically, suggesting again that s–s bonding dominates over d–d interactions. The cohesive energy was calculated at the GVB-RCI(3/6)*[SD_{s-s} + SD_{d-d}] level for all states and at the

(32) Martin, R. L.; Davidson, E. R. *Mol. Phys.* **1978**, *35*, 1713.
(33) Walch, S. P. *J. Chem. Phys.* **1987**, *87*, 6776.
(34) Cheng, P. Y.; Duncan, M. A. *Chem. Phys. Lett.* **1988**, *152*, 341.
(35) Balasubramanian, K.; Liao, M. Z. *Chem. Phys.* **1988**, *127*, 313.
(36) Rohlfing, E. A.; Valentini, J. J. *Chem. Phys. Lett.* **1986**, *126*, 113.
(37) Crumley, W. H.; Hayden, J. S.; Gole, J. L. *J. Chem. Phys.* **1986**, *84*, 5250.
(38) Walch, S. P.; Laskowski, B. C. *J. Chem. Phys.* **1986**, *84*, 2734.
(39) Morse, M. D. *Chem. Phys. Lett.* **1987**, *133*, 8.

TABLE VIII: Mulliken Populations for the 10 Lowest-lying Electronic States of Pt_3

	total valence electron configuration						Pt–Pt bond character, %					
	Pt_a[a]			Pt_b[b]			Pt_a[a]			Pt_b[b]		
state	d	s	p	d	s	p	d	s	p	d	s	p
$^5B_1$	8.91	1.01	0.17	8.92	0.87	0.12	0.2	9.9	2.3	13.9	28.1	1.8
$^5A_2$	8.91	1.02	0.19	8.93	0.87	0.13	0.5	9.0	2.3	13.1	29.0	2.0
$^3B_1$	8.91	0.99	0.19	8.94	0.85	0.13	0.5	8.7	2.6	11.6	30.4	2.1
$^3A_2$	8.91	1.01	0.19	8.93	0.87	0.13	0.2	9.2	2.6	12.0	30.1	1.9
$^5B_2$	8.92	0.98	0.19	8.94	0.84	0.14	1.6	9.2	2.4	12.9	28.6	1.9
$^3A_1$	8.96	0.97	0.19	8.93	0.86	0.13	1.5	8.0	2.6	12.0	29.9	2.0
$^3B_2$	9.74	0.40	0.06	8.96	0.83	0.09	2.9	14.3	2.9	4.9	33.3	1.7
$^1A_1$	9.72	0.40	0.06	8.95	0.83	0.09	3.4	14.8	3.0	4.9	32.8	1.7
$^5A_1$	8.95	0.72	0.22	8.93	0.95	0.15	10.6	26.3	1.7	4.8	23.5	2.5
$^5\Delta_g$	8.83	1.02	0.19	8.96	0.96	0.06	72.3	1.4	0.0	0.4	11.6	1.1

[a] Pt_a is the apex Pt atom. [b] Pt_b is a base Pt atom.

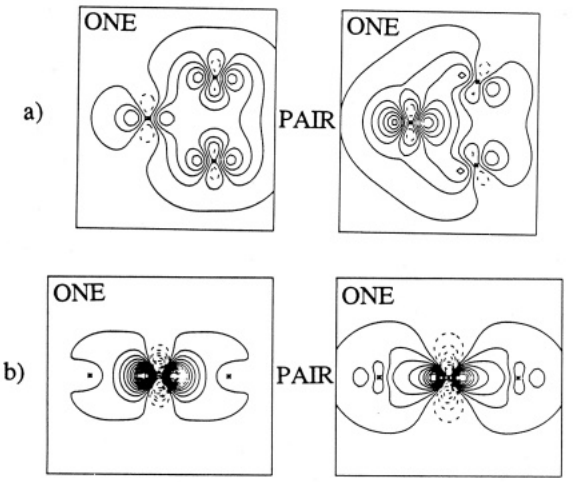

Figure 2. GVB one-electron orbitals for (a) the 6s–6s bond of the $^5A_1$ state at its optimum geometry (overlap = 0.78) and (b) the 6s–5d bond of the $^5\Delta_g$ state at its optimum geometry (overlap = 0.84). Contours range from −0.50 to 0.50 au, at intervals of 0.03 au.

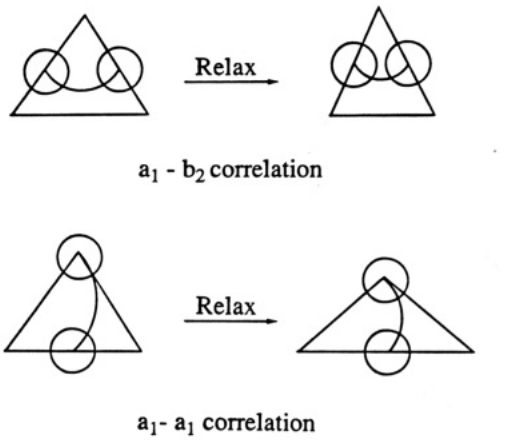

Figure 3. Different correlations lead to different geometric relaxations: (a) a_1–b_2 correlations favor acute triangles and (b) a_1–a_1 correlations favor obtuse triangles.

CCCI level for the "ground" $^3A_1$ state. We predict an atomization energy of 50.3 kcal/mol, which is almost certainly a lower bound on the actual bond energy.

We also see from Table VII that angular relaxations are very slight, with most states retaining angles slightly less than 60°, which strengthens the metal–metal interaction by increasing orbital overlap. Changes in the apex Pt–base Pt bond lengths are a little more dramatic, ranging from 2.79 to 2.98 Å. Not surprisingly, the shortest bond length is found for the $^1A_1$ state again, in order to maximize s–s and d–d overlap, while the longest apex to base bond is predicted for the least bound $^5A_2$ state. The triplet and quintet states have similar bond lengths because the only difference between these states is the intraatomic spin coupling on the apex Pt atom, which should not perturb the bond lengths very much. The very small angular distortions from equilateral triangles are an indication that the more angle dependent d and p electrons play no essential role in the formation of Pt_3. Indeed, the predominance of angular-independent s character can be seen in the Mulliken population analysis in Table VIII for the M–M bond. Mulliken population analysis also helps rationalize why the $^1A_1$ and $^3B_2$ states prefer to remain equilateral triangles, while the rest of the states distort to isosceles triangles. The $^1A_1$ and $^3B_2$ states have one d^{10}-like and two d^9s^1-like Pt atoms instead of three d^9s^1-like Pt atoms as in all other states (Table VIII). This results in a 6s-electron configuration of $(a_1)^2$ for $^1A_1$ and $^3B_2$, which does not give rise to a Jahn–Teller distortion.

Table IX displays the hybridization found for all other active orbitals for each state examined. In general, the open-shell orbitals and d–d bonds are pure d, with little sp mixing in. However, each state, except for $^3B_2$ and $^1A_1$ for the reasons stated above, has a 6s radical orbital that is generally localized on the apex Pt atom in order to avoid overlap with the Pt–Pt s–s bond that involves primarily the base Pt atoms (see Table VIII). This radical orbital mixes in up to ≅11% p character in all cases except for the $^5A_1$ and $^5\Delta_g$ states, where the p character is higher (12.4 and 15.7%, respectively) due to the nature of the molecular orbitals. The MOs in the latter two cases mix in p character on the central (apex) Pt atom to combine with antisymmetric combinations of 6s orbitals on the terminal (base) Pt atoms.

Among the seven states with isosceles triangle geometries, only the $^5A_1$ state has a shorter apex Pt–base Pt bond distance and wider apex angle than the equilateral triangle geometry. This is because the $^5A_1$ state prefers to utilize an a_1 orbital to correlate the s–s bond (Figure 2a), while all of the other bent states have one s–s bond preferentially described by a nearly doubly occupied a_1 combination of the 6s orbitals and a nearly empty b_2 correlating orbital (Figure 1 and Table IV). As illustrated in Figure 3, the latter case favors an elongation of the apex–base Pt distance and a contraction of the apex angle to increase overlap in the s–s bond. By contrast, the a_1 correlating orbital in the $^5A_1$ state can maximize overlap of its s–s bond by increase its apex angle beyond 60°. We emphasize that the choice of a_1–b_2 versus a_1–a_1 correlation of the s–s bond was not arbitrary: both were tried for each state and the lowest energy configuration was optimized.

The lowest lying linear state of Pt_3 is of $^5\Delta_g$ symmetry and has all three Pt atoms in d^9s^1 configurations. This is different from the $^5\Delta_u$ state of Ni_3 (its lowest lying Δ state), which has one d^8s^2 central atom and two d^9s^1 terminal atoms.[13] The state inversion is simply due to the atomic energy level ordering: for Pt atom, the d^8s^2 state is 14.7 kcal/mol higher than the d^9s^1 state, while for Ni atom, the d^8s^2 state is almost degenerate with the d^9s^1 ground state (only 0.69 kcal/mol higher). Therefore the transition from ground state d^9s^1 to d^8s^2 costs little promotional energy to form $^5\Delta_u$ Ni_3 but is significant for the formation of $^5\Delta_u$ Pt_3. Analysis of the bond character for the linear $^5\Delta_g$ state of Pt_3 shows that the metal–metal bonding here is dominated by formation of

TABLE IX: Mulliken Populations for All Other Active Orbitals in Each Low-Lying State of Pt_3[a]

			hybridization, %		
state	orb sym	atom	s	p	d
$^5B_1$	a_1	Pt_a	0.0	0.0	0.2
		Pt_b	2.2	0.0	47.7
	a_1[b]	Pt_a	61.4	10.3	1.6
		Pt_b	4.9	7.4	1.1
	a_2	Pt_a	0.0	0.0	99.8
		Pt_b	0.0	0.0	0.1
	b_2	Pt_a	0.0	0.0	0.2
		Pt_b	1.4	0.0	48.5
$^5A_2$	a_1	Pt_a	0.0	0.0	0.2
		Pt_b	1.9	0.0	48.0
	a_1[b]	Pt_a	65.8	10.2	1.1
		Pt_b	4.1	6.4	1.0
	b_1	Pt_a	0.0	0.0	99.5
		Pt_b	0.0	0.1	0.2
	b_2	Pt_a	0.0	0.0	0.2
		Pt_b	1.2	0.0	48.6
$^3B_1$	a_a/b_2[c]	Pt_a	0.0	0.0	0.1
		Pt_b	2.0	0.0	48.0
	a_1[b]	Pt_a	67.3	10.9	1.1
		Pt_b	3.4	6.1	0.8
	b_1	Pt_a	0.0	0.0	99.5
		Pt_b	0.0	0.1	0.1
$^3A_2$	a_1/b_2[c]	Pt_a	0.0	0.0	0.1
		Pt_b	2.1	0.0	47.8
	a_1[b]	Pt_a	64.6	10.8	1.6
		Pt_b	3.9	6.8	0.8
	a_2	Pt_a	0.0	0.0	99.8
		Pt_b	0.0	0.0	0.1
$^5B_2$	a_1	Pt_a	0.2	0.1	4.3
		Pt_b	2.2	0.0	45.5
	a_1	Pt_a	3.0	0.1	91.9
		Pt_b	0.1	0.0	2.4
	a_1[b]	Pt_a	62.4	11.2	2.1
		Pt_b	4.3	6.9	1.0
	b_2	Pt_a	0.0	0.0	0.2
		Pt_b	1.4	0.0	48.5
$^3A_1$	a_1/b_2[c]	Pt_a	0.0	0.0	0.0
		Pt_b	2.1	0.0	47.9
	a_1	Pt_a	2.9	0.2	96.4
		Pt_b	0.2	0.0	0.1
	a_1[b]	Pt_a	66.0	11.2	1.9
		Pt_b	3.4	6.3	0.8
$^3B_2$	a_1/a_1[d]	Pt_a	1.4	0.0	92.4
		Pt_b	1.6	0.9	0.7
	a_1	Pt_a	0.0	0.0	0.5
		Pt_b	2.5	0.0	47.3
	b_2	Pt_a	0.0	0.0	0.3
		Pt_b	2.0	0.1	47.8
$^1A_1$	a_1/b_2[c]	Pt_a	0.0	0.0	0.4
		Pt_b	2.3	0.0	47.5
	a_1/a_1[d]	Pt_a	1.2	0.0	91.9
		Pt_b	1.9	0.9	0.7
$^5A_1$	a_1	Pt_a	4.0	0.0	77.1
		Pt_b	0.6	0.1	8.8
	a_1	Pt_a	0.4	0.1	18.5
		Pt_b	1.5	0.0	39.0
	b_2	Pt_a	0.0	0.0	0.0
		Pt_b	1.5	0.0	48.5
	b_2[b]	Pt_a	0.0	12.4	1.0
		Pt_b	32.1	9.3	1.9
$^5\Delta_g$	δ_g	Pt_a	0.0	0.0	0.0
		Pt_b	0.0	0.0	50.0
	δ_g	Pt_a	0.0	0.0	100.0
		Pt_b	0.0	0.0	0.0
	σ_u[b]	Pt_a	0.0	15.7	0.0
		Pt_b	42.0	0.2	0.0
	δ_u	Pt_a	0.0	0.0	0.0
		Pt_b	0.0	0.0	50.0

[a] Pt–Pt s–s bond populations are shown in Table VIII (and thus are excluded here). Pt_a = apex Pt atom. Pt_b = base Pt atom. [b] Singly occupied s-like radical orbital. [c] d–d bond. [d] d lone pair on a d^{10}-like Pt atom.

a three-center, two-electron bond (Figure 2b), in which the central atom uses its d_{z^2} orbital to interact with the two terminal Pt atoms s orbitals. In addition, the Pt–Pt bond switches from mostly s-like to mostly d-like upon conversion from a bent to a linear structure (Table VIII). All other linear states examined were at least 10 kcal/mol higher in energy based on CI calculations used to screen states of interest (section II).

Our calculations are roughly consistent with the photoelectron spectrum of Pt_3^-,[15] which consists of two distinct envelopes (each containing structure) at electron binding energies ranging from 1.87 to 2.02 eV. Our calculations suggest that the high density of Pt_3 electronic states is at least partially responsible for the narrow distribution of photodetached electrons. The nearly filled d shell on Pt makes it impossible for the metal–metal bonds to shorten, because of interatomic repulsive interactions. The large bond distances cause interatomic d–d coupling energies to be very small, leading to the dense manifold of states. Our results also provide theoretical support for Eberhardt et al.'s suggestion[17] that for platinum trimer, a linear structure is close in energy to triangular structures, based on the unusually large broadening observed for the 4f core-level photoemission spectrum. However this broadening may simply be due to the large number of nearly isoenergetic electronic states all with distinct geometries that perturb the core levels in their own way. We also cannot rule out the importance of vibronic coupling, however, since we find all of these potential surfaces to be very flat in the region of the minimum.

Examining the ab initio results for Ni_3, Pd_3, and Pt_3, we see that all three trimers are predicted to have many states lying close in energy, i.e., Ni_3 has six states lying within 3.9 kcal/mol;[13] Pd_3 has at least 15 states within 10.4 kcal/mol;[16] and Pt_3 has 10 states within 6.6 kcal/mol, resulting from various combinations of different low-lying atomic states. The atom's ground and first excited state electronic structure largely determines this combination. For example, the ground states for Ni, Pd, and Pt are d^9s^1 (^3D), d^{10} (^1S), and d^9s^1 (^3D), respectively, where the first excited states are d^8s^2 Ni (^3F, 0.69 kcal/mol up), d^9s^1 Pd (^3D, 21.9 kcal/mol up), and d^{10} Pt (^1S, 11.1 kcal/mol up). Thus Ni_3 arises from Ni (d^9s^1) + Ni(d^8s^2), Pd_3 is a Pd (d^9s^1)–Pd (d^{10}) mixture, and Pt_3 involves Pt atoms in either the d^9s^1 or d^{10} states, with d^9s^1 dominating. The predominance of the d^9s^1 local electronic configuration at each metal center and hence a predominance of s–s bonding leads to a preference for bent structures for all three noble metal trimers, just as in the coinage and alkali-metal trimers, where s–s bonding is the only choice.[32-39] Linear structures are competitive for Ni_3 and Pt_3 because the middle metal atom can readily adopt either a d^8s^2 or a d^9s^1 configuration, whereas Pd_3 incurs higher atomic promotional costs to adopt a linear structure. Finally, our predicted lower bound for the adiabatic atomization energy for Pt_3 of 50.3 kcal/mol is close to that predicted for Pd_3 (53 kcal/mol) at a similar level of calculation.[16] Thus the metal–metal bonds in Pd and Pt clusters may be quite similar, perhaps due to a balance between electronic promotion and electron repulsion effects. In particular, Pd atoms have less core–core electron repulsion than Pt atoms, allowing Pd–Pd bonds to be slightly shorter than Pt–Pt bonds (cf. ref 16 and this work). On the other hand, Pd has a nonbonding d^{10} ground state that must be promoted to the d^9s^1 state in order to form the cluster, while Pt has a bonding d^9s^1 ground state and thus incurs no promotional costs. These two effects may balance, leading to similar cohesive energies.

IV. Conclusions

In this investigation, we find 10 low-lying electronic states of Pt_3 within 6.6 kcal/mol. The $^1A_1$ and $^3B_2$ states, arising from one d^{10} and two d^9s^1 Pt atoms, have equilateral triangle structures, because their s-electron configuration dictates that no Jahn–Teller distortion from D_{3h} symmetry will occur. The $^3A_1$, $^5B_2$, $^3A_2$, $^3B_1$, $^5A_2$, and $^5B_1$ states, comprised of three d^9s^1 atoms, exhibit isosceles triangle geometries with apex angles <60° due to Jahn–Teller distortions and the drive for increased metal–metal bond overlap. The $^5A_1$ state, also consisting of d^9s^1 Pt atoms, has an isosceles triangle structure with an apex angle >60° due to the change in

its electron correlation preferences. The $^5\Delta_g$ state is linear with three d^9s^1 Pt atoms involved in a three-center two-electron bond that is primarily d-like on the center Pt and s-like on the terminal Pt atoms. The metal-metal bonding is dominated by delocalized s-s interactions for the bent clusters, with the valence d electrons preferring to remain localized on each metal center. s-d hybridization does play a role in maximizing the overlap in what is primarily a 6s-6s bond (about 15-30% 5d) in all bent states, while we find s-p hybridization to be of negligible importance. The cohesive energy of Pt trimer ($^3A_1$) with respect to three separated ground-state Pt atoms (^3D) is found to be at least 50.3 kcal/mol.

Acknowledgment. This work was supported by the Office of Naval Research (Grant No. N00014-89-J-1492) and partially by a grant from Aerojet Electrosystems. E.A.C. also acknowledges support from the National Science Foundation and the Camille and Henry Dreyfus Foundation through their Presidential Young Investigator and Distinguished New Faculty Award Programs.

Registry No. Pt_3, 110743-43-6.

Steric and Stereoelectronic Effects on Metal Ion Incorporation into Picket Fence Porphyrins in Homogeneous Solution: The Relationship of Molecular Conformation to Reactivity[1]

David C. Barber, David S. Lawrence, and David G. Whitten*

Department of Chemistry, University of Rochester, Rochester, New York 14627-0216
(Received: February 27, 1991; In Final Form: September 20, 1991)

Rate constants for the incorporation of Cu(II) and Zn(II) using the perchlorate salts were measured for the four atropisomers of C_2 and C_{16} derivatives of *meso*-tetrakis(*o*-alkylamidophenyl)porphyrin, the "picket fence" porphyrins (PFPs) in *N,N*-dimethylformamide (DMF). A 156-fold variation in rate constants is noted for Cu(II) incorporation into the 25 PFPs studied in DMF which are 56.5-8800 times less reactive than *meso*-tetraphenylporphyrin (TPP). For Cu(II) incorporation, the reactivity order is 4,0 > 3,1 > cis 2,2 > trans 2,2 in all cases. The span of metalation rate constants for individual isomers as a function of side chain length follows the opposite order, consistent with increasing steric exclusion of metal ion as the number of substituents (0-2) about the less hindered face of the porphyrin increases. A 2.2×10^5-fold range of facial metalation rate constants calculated for TPP and the PFPs indicates that metalation of the 4,0 isomer occurs predominantly (>99%) from the unsubstituted face. Increased perpendicularity between the phenyl rings and the porphyrin core with increasing side chain bulk, attributed to (1) steric interactions between ortho substituents and the porphyrin core and (2) transannular side chain interactions, is postulated to result in enhanced core rigidity for the 4,0 isomer and consequent decreased metalation rates. This postulate is supported by ^1H NMR and UV-visible spectral data for the set of compounds studied, relative basicities, and molecular models. For the 4,0 isomer, whose metalation is controlled by such stereoelectronic factors, side chain branching more effectively inhibits metalation (range of $k_{Cu^{2+}} = 4.7\ M^{-1}\ s^{-1}$) than linear side chain extension (range of $k_{Cu^{2+}} = 2.2\ M^{-1}\ s^{-1}$). The results of this study are relevant to the spectroscopy, chemistry, and solution structure of tetraarylporphyrins.

Introduction

Extensive mechanistic studies of metal ion incorporation performed under various conditions with a wide variety of metal ions using natural and synthetic, water soluble and water insoluble free base porphyrins reveal that a variety of factors influence the rate of porphyrin metalation.[2-9] Controlling factors of metalation include (1) solvent composition, (2) ligands attached to the metal ion center, (3) solvent or ligand exchange rates of the metal ion, (4) metal ion coordination geometry, (5) ionic strength, (6) total porphyrin charge, (7) the location of porphyrin charge with respect to the porphyrin center, (8) Hammett substituent constants of groups attached to the porphyrin, (9) deformability of the macrocyclic core, (10) accessibility of pyrrole nitrogen atoms to the

CHART I: Picket Fence Porphyrin Structures and Atropisomer Representations

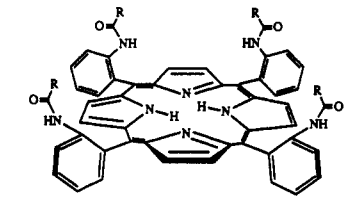

-R	Abbreviation
$-CH_3$	TAc
$-C_2H_5$	TPro
$-C_3H_7$	TBu
$-C_5H_{11}$	THex
$-C_6H_{13}$	THept
$-C_7H_{15}$	TOct
$-C_9H_{19}$	TDec
$-C_{15}H_{31}$	THA
$-CH(CH_3)_2$	TiBu
$-C(CH_3)_3$	TPiv

(1) Taken in part from the doctoral dissertation of David C. Barber, University of Rochester, 1989.
(2) Lavallee, D. K. *Coord. Chem. Rev.* **1985**, *61*, 55.
(3) Berezin, B. D. *Coordination Compounds of Porphyrins and Phthalocyanines*; John Wiley and Sons: New York, 1981.
(4) Longo, F. R.; Brown, E. M.; Rau, W. G.; Adler, A. D. In *The Porphyrins*; Dolphin, D., Ed.; Academic Press: New York, 1978; Vol. 5, pp 459-481.
(5) Hambright, P. In *Porphyrins and Metalloporphyrins*; Smith, K. M., Ed.; Elsevier: Amsterdam, 1975; pp 233-278.
(6) Schneider, W. *Struct. Bonding (Berlin)* **1975**, *23*, 123.
(7) Hambright, P. *Coord. Chem. Rev.* **1971**, *6*, 247.
(8) Falk, J. E., Lemberg, R., Morton, R. K., Eds. *Haematin Enzymes*; Pergamon: London, 1961.
(9) Falk, J. E. *Porphyrins and Metalloporphyrins*; Elsevier: Amsterdam, 1964; pp 35-40.

0022-3654/92/2096-1204$03.00/0